Gas Separation by Permeators with High-Flux Asymmetric Membranes

The permeation behavior of the high-flux asymmetric membrane differs from that of the conventional symmetric membrane. A calculation method for predicting the gas separation performance of a permeator with asymmetric membrane is presented. The model takes into account the permeate pressure drop and is applicable to both hollow-fiber and spiral-wound modules. The effect of permeate-feed flow pattern on module performance is analyzed. It is shown that for the high-flux asymmetric membrane, the countercurrent flow pattern is not necessarily always the preferred operating mode. The mathematical model is verified by large-scale field pilot-plant experiments for helium recovery from natural gas using large hollow-fiber modules (220 m^2/unit).

C. Y. PAN

Alberta Research Council
Edmonton, Alberta, Canada

SCOPE

The conventional symmetric membrane has a homogeneous structure with uniform permeation properties across its thickness. This type of membrane has not been widely used for gas separation mainly due to low rates of permeation imposed by the membrane thickness required for maintaining membrane integrity and strength. Recent development of asymmetric membranes, however, has made membrane permeation an important unit operation for gas separation. The membrane consists of an ultrathin skin and a porous supporting layer with negligible resistance to gas flow. The skin, which acts as the separation barrier, is highly permeable due to its thinness. This permits the use of highly selective polymers with inherently poor permeability for specific gas separation. The presence of the porous supporting layer, however, renders the permeation behavior of the asymmetric membrane somewhat different from that of the familiar symmetric membrane. A calculation method for predicting the performance of a permeator with the high-flux asymmetric membrane is presented. Both hollow-fiber and spiral-wound modules are considered. The effect of flow pattern on the performance of the asymmetric membrane is found to be significantly different from that of the symmetric membrane. Laboratory and pilot-plant data are presented to substantiate the mathematical model.

CONCLUSIONS AND SIGNIFICANCE

The porous supporting layer of the asymmetric membrane prevents the mixing of permeate fluxes of varying compositions on the membrane skin surface. Consequently, the asymmetric membrane always gives rise to cross-flow type of permeation regardless of the flow pattern and direction of the bulk permeate stream flowing outside the porous layer. It is this characteristic that sets the permeation behavior of the asymmetric membrane apart from the conventional symmetric membrane.

It is shown that, for the asymmetric membrane with narrow permeate flow path such as hollow fibers, the permeate pressure build-up is strongly dependent on the feed-permeate (the bulk stream) flow pattern. The countercurrent mode has the lowest permeate pressure build-up but the feed flow is in the undesirable direction in relation to the permeate pressure build-up. The cocurrent pattern, on the other hand, has the desirable direction of feed flow relative to the permeate pressure build-up but the permeate pressure build-up is excessive. The net effect of the permeate pressure build-up and the feed flow direction is that the feed-permeate flow pattern has little effect on the membrane performance and that the countercurrent pattern is not necessarily always the preferred operating mode.

The mathematical model presented here for calculating the performance of permeators with the high-flux asymmetric membrane has been verified by the field pilot-plant experiments for helium recovery from natural gas using large hollow-fiber modules. The model is applicable to both hollow-fiber and spiral-wound modules.

MATHEMATICAL MODEL ON ASYMMETRIC-MEMBRANE PERMEATION

The anisotropic structure of the asymmetric membrane renders its permeation behavior somewhat different from that of the symmetric membrane. The porous supporting layer will generally prevent the mixing of local permeate fluxes of varying concentrations on the permeate-side of the membrane skin surface, regardless of the flow direction of the bulk permeate stream outside the porous layer. This characteristic is shared by the symmetric membrane only when the permeate and feed are in cross-flow pattern. In other words, the asymmetric membrane always gives rise to cross-flow permeation irrespective of the feed and bulk permeate flow pattern. The lack of local permeate mixing on the membrane surface will have a significant effect on the gas separation efficiency of the membrane as the permeation driving force is directly dependent on the conditions of the gas on both sides of the membrane *surface*.

For the symmetric membrane, the performance of the membrane for gas separation is strongly dependent on the feed-per-

Alberta Research Council Contribution #1211

meate flow pattern (countercurrent, cocurrent or cross-flow), and various calculation methods have been reported in the literature (Blaisdell and Kammermeyer, 1972, 1973; Hwang and Kammermeyer, 1975; Naylor and Backer, 1955; Oishi et al., 1961; Pan and Habgood, 1974, 1978a, 1978b; Stern, 1972; Thorman et al., 1975; Walawender and Stern, 1972; Weller and Steiner, 1950a, 1950b). Some of these models take into account the feed or permeate pressure drop in the membrane module. For the cross-flow pattern, an analytical solution was first obtained by Weller and Steiner (1950a, b). The solution is based on no local permeate mixing on the membrane surface, and therefore should be applicable to the high-flux asymmetric membrane in any flow pattern, provided that the permeate and feed pressures are both constant. None of the existing calculation methods, however, is applicable to an asymmetric-membrane module with appreciable permeate pressure drop caused by high permeate flux. In the following, calculation methods are presented for the permeation of a binary gas mixture through the asymmetric membrane with significant permeate pressure drop in cocurrent, countercurrent or cross-flow pattern. Here the "flow pattern" refers to the relative flow directions of the feed and the *bulk* permeate stream flowing outside the porous supporting layer of the membrane. The model is applicable to the spiral-wound module and the hollow-fiber permeator with feed flow outside of the fiber.

Assumptions

The following mathematical formulation for the permeation of the asymmetric membrane is based on these assumptions:

1. The feed gas is on the skin side of the asymmetric membrane.
2. No mixing of permeate fluxes of different compositions occurs inside the porous supporting layer of the membrane.
3. The porous supporting layer has negligible resistance to gas flow, and diffusion along the pore path is insignificant due to high permeate flux.
4. The membrane permeabilities are independent of pressure and concentration.
5. Feed gas pressure drop is negligible.
6. The permeate flow inside the fiber and the spiral-wound leaf is governed by the Hagen-Poiseuille equation. This is a reasonable assumption based on the analysis of laminar flow in a channel with porous walls (Berman, 1953).
7. In the case of hollow-fiber membrane, the deformation of the fiber under pressure is assumed to be negligible. This is reasonable since the estimated displacement of the inside diameter of a typical cellulose acetate fiber with $D_o/D_i = 2.5$ under 6,870 kPa external pressure is only 0.9% based on the Lame' equations for a thick-walled cylinder with 1.4×10^6 kPa modulas of elasticity and 0.5 Poisson ratio.

Cocurrent and Countercurrent Flow Pattern

Figure 1 illustrates a single asymmetric hollow fiber operating in the cocurrent mode with feed flow outside the fiber. Here it is important to note that the concentration of the permeate leaving the membrane skin surface y' is generally different from that of the bulk permeate stream outside the porous layer y, except at the closed end of the fiber where they are identical. The following formulation is set up in terms of the cocurrent flow pattern, but the resulting equations are also applicable to the countercurrent pattern if negative values are assigned to the feed-side flows.

Permeation

$$\frac{d(Ux)}{dl} = -\pi D_o N(Q_a/d)(Px - py') \tag{1}$$

$$\frac{d[U(1-x)]}{dl} = -\pi D_o N(Q_b/d)[P(1-x) - p(1-y')] \tag{2}$$

$$\frac{d(Ux)}{dU} = y' \tag{3}$$

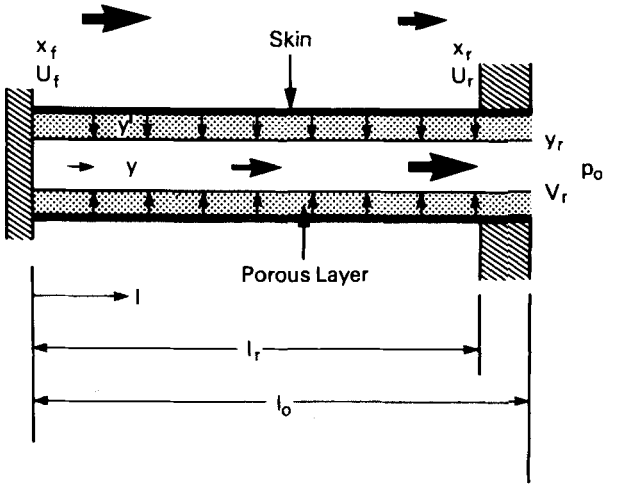

Figure 1. Asymmetric hollow-fiber membrane operating in the cocurrent mode with feed flow outside the fiber.

Permeate Pressure Drop

$$\frac{dp^2}{dl} = \frac{-256RT\mu V}{\pi g_c D_i^4 N} \tag{4}$$

Material Balance

$$U + V = U_f \tag{5}$$

$$Ux + Vy = U_f x_f \tag{6}$$

Equations 1 and 2 show that the permeation driving force across the membrane is dependent on the feed-side concentration x and the local permeate concentration y'. Equation 3 states that the mole fraction of a component in the permeate leaving the membrane surface is equal to the flow fraction of the same component in the permeate flux through the membrane. Equation 4 is the Hagen-Poiseuille equation in a differential form. The integration of this equation must take into account the variation of permeate flow (V) along the fiber. It is significant to note that the bulk permeate concentration y is used only in the material balance Eqs. 5 and 6. In the following, Eqs. 1–6 are transformed into convenient forms for mathematical solution.

With the aid of Eq. 3, the ratio of Eqs. 1 and 2 becomes

$$\frac{y'}{1-y'} = \frac{\alpha(x - \gamma y')}{1 - x - \gamma(1-y')} \tag{7}$$

Solving for y' from Eq. 7 yields

$$y' = \frac{1 + (\alpha-1)(\gamma+x) - \sqrt{[1+(\alpha-1)(\gamma+x)]^2 - 4\gamma\alpha(\alpha-1)x}}{2\gamma(\alpha-1)} \tag{8}$$

Solving for U and V from Eqs. 5 and 6 gives

$$\frac{U}{U_f} = \frac{y - x_f}{y - x} \tag{9}$$

$$\frac{V}{U_f} = \frac{x_f - x}{y - x} \tag{10}$$

Equation 3 may be written as

$$\frac{dU}{dx} = \frac{U}{y' - x} \tag{11}$$

With the aid of Eq. 5, the differentiation of Eq. 6 with respect to x yields

$$\frac{dy}{dx} = \frac{y - x}{U_f - U}\frac{dU}{dx} - \frac{U}{U_f - U} \tag{12}$$

Substituting Eqs. 9 and 11 into Eq. 12, we obtain

$$\frac{dy}{dx} = \frac{(y - x_f)(y' - y)}{(x - x_f)(y' - x)} \tag{13}$$

where y' in the equation can be expressed in terms of x by Eq. 8. With the aid of Eqs. 9 and 11, the sum of Eqs. 1 and 2 becomes

$$\frac{dS}{dx} = \frac{y - x_f}{(x - y)(y' - x)[\alpha(x - \gamma y') + 1 - x - \gamma(1 - y')]} \tag{14}$$

Substituting Eq. 10 into Eq. 4 yields

$$\frac{d\gamma^2}{dS} = \frac{A(\mu/\mu_b)(x_f - x)}{x - y} \tag{15}$$

where

$$S = \pi D_o l N (Q_b/d)(P/U_f) \tag{16}$$

$$A = \frac{256\mu_b RTU_f^2}{\pi^2 g_c (Q_b/d) P^3 D_o D_i^4 N^2} \tag{17}$$

Over the inactive length of the fiber imbedded in the tubesheet, Eq. 15 may be integrated to yield

$$\gamma_r^2 = \gamma_o^2 + \frac{A(\mu_r/\mu_b)(x_f - x_r)(S_r - S_o)}{(x_r - y_r)(D_t/D_i)^4} \tag{18}$$

where D_t is the inside diameter of the inactive fiber.

Equations 1–6 have now been transformed into Eqs. 8–10 and 13–15. Numerical methods are necessary for integrating the simultaneous differential Eqs. 13–15.

Calculation Problem. For a given hollow fiber module with specified operating pressures (feed-side pressure and permeate pressure at fiber opening), there are eight variables (x_f, x, y, y', U_f, U, V and p) to satisfy six equations (Eqs. 8–10 and 13–15); therefore, any two of these variables may be specified. Regardless of which two variables are specified, the calculation problem is always of the boundary value type; the boundary conditions at either end of the fiber cannot be sufficiently specified to initiate the integration of Eqs. 13–15. The trial and error "shooting method" may be used to obtain the solution. However, for the typical calculation problem with specified feed and residue concentrations, the iteration method described below will simplify the calculation. Such a calculation problem is often encountered in the design of an ideal permeation cascade. In an ideal cascade, the residue concentration in the first stage is usually specified according to the desired recovery, and the feed and residue concentrations in each of the subsequent stages are set equal to the permeate and feed concentrations of the preceding stage, respectively. With operating pressures, feed and residue concentrations specified, the boundary conditions for the differential Eqs. 13–15 are as follows:

$x = x_f$	$y = y' = y'_f(x_f, \gamma_f)$ (Eq. 8)	at $S = 0$
$x = x_r$	$\gamma = \gamma_o$	at $S = S_o$

Where γ_f is an unknown yet to be determined. At $S = 0$, Equation 13 appears to be indeterminate, but its value can be determined by L'Hopital's rule, and is given by:

$$(dy/dx)_f = (y'_f - x_f)[\alpha - (\alpha - 1)y'_f]/\{\alpha(1 - x_f)(x_f - \gamma_f y'_f) - x_f[1 - x_f - \gamma_f(1 - y'_f)] - (y'_f - x_f)[(\alpha - 1)(2\gamma_f y'_f - x_f - \gamma_f) - 1]\} \tag{19}$$

Calculation Procedure. The calculation method presented here is an iteration procedure for solving Eqs. 13–15 with the above boundary conditions. The essence of the method is using an arbitrarily prescribed permeate pressure profile inside the fiber to determine an approximate concentration profile by Eqs. 13 and 14, which in turn is used to generate a new pressure profile by Eq. 15. An improved concentration profile is then obtained from the corrected pressure profile, and vice versa, until both profiles converge to their respective limits. The advantage of this calculation procedure is that the simultaneous Eqs. 13–15 can be integrated separately and sequentially. The algorithm for this iteration method is described below.

(1) As a first approximation, assume the permeate pressure is independent of x and the permeate/feed pressure ratio γ is everywhere equal to γ_o (i.e., assuming no permeate pressure build-up).

(2) With the aid of this $x - \gamma$ relation, integrate Eq. 13 numerically (e.g., Runge-Kutta method) from x_f to x_r to obtain the $x - y$ relation and the permeate concentration at the fiber outlet, y_r. This relation is in turn used to integrate Eq. 14 to yield the $x - S$ relation and S_r (the value of S at $x = x_r$). Calculate the values of U_f and A by Eqs. 16 (setting $S = S_r$ and $l = l_r$) and 17, respectively.

(3) Calculate γ_r at the end of the active fiber by Eq. 18, then utilizing the $x - y - S$ relation obtained in Step (2), integrate Eq. 15 from $S = S_r$ to $S = 0$ to generate a new $\gamma - S$ relation, and hence a new $x - \gamma$ relation. Obtain a corrected $x - \gamma$ relation by averaging the γ's in the old and new $x - \gamma$ profiles. (The averaging procedure will prevent the occurrence of oscillation of the pressure and concentration profiles in the iterative calculations.)

(4) Repeat Steps (2) and (3) until y_r converges to the desired accuracy, then calculate U_r and V_r by Eqs. 9 and 10, respectively. This completes the calculation. Generally 0.5% accuracy for y_r can be obtained within four iterations.

Cross-Flow Pattern

Figure 2 illustrates the feed and permeate flows in an extended membrane leaf of a spiral-wound module. The permeate and feed are in the cross-flow mode. A long membrane leaf coupled with high permeate flux will give rise to significant permeate pressure build-up inside the leaf. The pressure variation on the permeate side of the membrane will cause the concentrations and flows to vary in both the feed and permeate flow directions. This two-dimensional calculation problem can be greatly simplified if the permeate pressure is assumed to vary only in the permeate flow direction, i.e., the l-direction shown in Figure 2. This is a reasonable assumption for a spiral-wound module with short-leaf width and is the basis of the following formulation.

Permeation

$$\left[\frac{\partial(ux)}{\partial w}\right]_l = -2(Q_a/d)(Px - py') \tag{20}$$

$$\left[\frac{\partial[u(1 - x)]}{\partial w}\right]_l = -2(Q_b/d)(Px - py') \tag{21}$$

$$\frac{d(ux)}{du} = y' \tag{22}$$

Permeate Pressure Drop

$$\frac{d(p^2)}{dl} = \frac{-2RT\mu V}{g_c W t B} \tag{23}$$

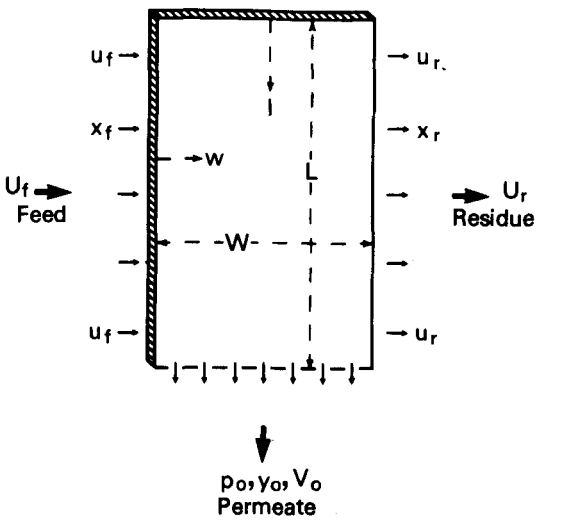

Figure 2. Permeation through a membrane leaf of a spiral-wound module. The leaf consists of two pieces of membrane separated by spacing materials and sealed on three edges. The unsealed edge is the permeate outlet.

Material Balance

$$\frac{dV}{dl} = u_f - u_r \tag{24}$$

$$\frac{d(Vy)}{dl} = u_f x_f - u_r x_r \tag{25}$$

The numeral 2 in Eqs. 20 and 21 is due to the fact that each membrane leaf has two pieces of membranes (one on each side). Equation 23 is Darcy's Law and B is the permeability of the spacing materials inside the membrane leaf. The local residue flow and concentration, u_r and x_r, in Eqs. 24 and 25 are not constant and vary with l. The y in Eq. 25 is the average permeate concentration (over the width W) at a given l.

Since the permeate pressure is assumed to vary only in the direction of l as shown in Figure 2, the permeate pressure in Eqs. 20 and 21 can be treated as a constant if the integration is carried out in the direction of w. The Weller and Steiner (1950a, b) solution for the cross-flow pattern with constant permeate pressure will apply here. A similar solution in simpler forms as obtained by Pan and Habgood (1978a) will be used here and is given below.

$$\left(\frac{y'}{y'_f}\right)^{[\gamma(\alpha-1)+1]/[(\alpha-1)(1-\gamma)]}\left(\frac{1-y'}{1-y'_f}\right)^{[\gamma(\alpha-1)-\alpha]/[(\alpha-1)(1-\gamma)]} \times \left(\frac{\alpha-(\alpha-1)y'}{\alpha-(\alpha-1)y'_f}\right) \tag{26}$$

$$2W(Q_b/d)(P/u_f) = \frac{1}{\alpha(1-\gamma)}\{\alpha-(\alpha-1)y'_f - [\alpha-(\alpha-1)y'_r](u_r/u_f) - (\alpha-1)\int_{y'_f}^{y'_r}(u/u_f)\gamma dy'\} \tag{27}$$

where y' is a function of x as given by Eq. 8. Equations 26 and 27 are only part of the solution to the calculation problem, and give only the *local* residue concentration x_r (Eq. 27) and flow u_r (Eq. 26) as a function of *local* permeate pressure γ which is yet to be determined by Eqs. 23–25. Equations 23–25 may be written in the following dimensionless forms:

$$\frac{d\gamma^2}{dh} = -c\left(\frac{\mu}{\mu_b}\right)\theta \tag{28}$$

$$\frac{d(\theta y)}{dh} = x_f - x_r\left(\frac{u_r}{u_f}\right) \tag{29}$$

$$\frac{d\theta}{dh} = 1 - \frac{u_r}{u_f} \tag{30}$$

where

$$h = \frac{l}{L} \tag{31}$$

$$\theta = \frac{V}{Lu_f} = \frac{V}{U_f} \tag{32}$$

$$c = \frac{2RT\mu_b LU_f}{g_c WtBP^2} \tag{33}$$

Equations 8 and 26–30 are now the governing equations for the spiral-wound membrane module. These equations may also be applicable to the hollow fiber module in cross flow pattern, e.g., a module with a porous central feed tube. In this case, Figure 2 may be looked upon as a collection of fibers aligned lengthwise in the direction of l, and Eqs. 27 and 33 are modified with the following substitutions:

$$2W = \pi D_o N \tag{34}$$

$$128WtB = \pi D_i^4 N \tag{35}$$

Here the permeate pressure calculated by Eq. 28 is the average pressure profile inside the fiber. The actual pressure profile will vary somewhat from fiber to fiber due to lack of permeate-flow communication among individual fibers.

Calculation Problem. As in other flow patterns, for a given module in the cross-flow mode with fixed operating pressures, only two of the flow rates and/or concentrations may be specified. The calculation problem for the cross-flow pattern, however, is generally more complicated than the countercurrent or cocurrent flow pattern mainly because the local residue flow and concentration in the cross-flow mode vary with position. The simplest calculation problem is one with specified feed flow and feed concentration. In this case, a simple iterative calculation method may be used to obtain the solution of Eqs. 28–30. The method of solution is described below.

Calculation Procedure. For a given module with fixed membrane dimensions (L,W), operating pressures (P,p_o) and feed conditions (U_f,x_f), the local residue concentration and flow at a given l (x_r and u_r) depend only on the permeate/feed pressure ratio γ according to Eqs. 26 and 27 (where the y'_f and y'_r are related to x_f and x_r, respectively, by Eq. 8). Hence, the righthand sides of Eqs. 29 and 30 are functions of γ only. Therefore, with an assumed permeate pressure profile (i.e., a $\gamma - h$ relation), Eqs. 29 and 30 can be integrated to yield a $\theta - y - h$ relation. This relation can be used to generate a corrected $\gamma - h$ relation by Eq. 28 which in turn is used to obtain an improved $\theta - y - h$ relation by Eqs. 29 and 30. The iteration procedure may be outlined as follows:

(1) As a first approximation, assume the permeate/feed pressure ratio is everywhere equal to γ_o.

(2) With the aid of this $\gamma - h$ relation and Eqs. 26–27, integrate Eqs. 29 and 30 numerically from $h = 0$ (where $\theta = \theta y = 0$) to $h = 1$ to obtain a $\theta - y - h$ relation and the permeate outlet concentration y_o.

(3) Utilizing the $\theta - y - h$ relation obtained in Step (2), integrate Eq. 28 from $h = 1$ (where $\gamma = \gamma_o$) to $h = 0$ to obtain a new $\gamma - h$ relation. Obtain a corrected $\gamma - h$ relation by averaging the γ's in the new and old $\gamma - h$ profiles. (The averaging procedure will eliminate the occurrence of oscillation in the iterative calculation.)

(4) Repeat Steps (2) and (3) until y_o converges to the desired accuracy. The permeate outlet flow is then calculated from the θ value at $h = 1$ by Eq. 32. The average residue flow and concentration can be calculated by material balance over the entire membrane module.

ANALYSIS ON EFFECT OF FLOW PATTERN

It has long been known that the feed-permeate flow pattern has a great effect on the performance of the symmetric membrane. The countercurrent pattern is always the best, and the cross-flow pattern is always intermediate with respect to membrane area, permeate enrichment or product recovery. It is shown here, however, that for permeators with asymmetric membranes, the effect of feed-permeate (bulk stream) flow pattern is greatly reduced and the preferred flow pattern is not always necessarily the countercurrent mode.

For asymmetric membranes with uniform permeate pressure, flow pattern has no effect on the membrane performance. For permeators with small hollow fibers or long spiral-wound leaf, however, the permeate pressure build-up in the flow path is often very significant. The magnitude and profile of the permeate pressure build-up is shown below to be strongly dependent on the feed-permeate flow pattern. Hence, the effect of flow pattern on the performance of asymmetric membrane is through its influence on the permeate pressure profile.

To understand the effect of flow pattern on the membrane performance, we first examine the effect of a given permeate pressure variation on the membrane gas separation efficiency, leaving aside for the moment the effect of flow pattern on the permeate pressure profile. Figure 3 shows two permeators in three different operating modes with various permeate pressure configurations. The permeate pressure in the permeator is assumed to be uniform, but different for each permeator (either 687 kPa or 172 kPa). In Mode A, the feed gas enters the unit with a lower permeate pressure, and the residue is treated by the unit with a

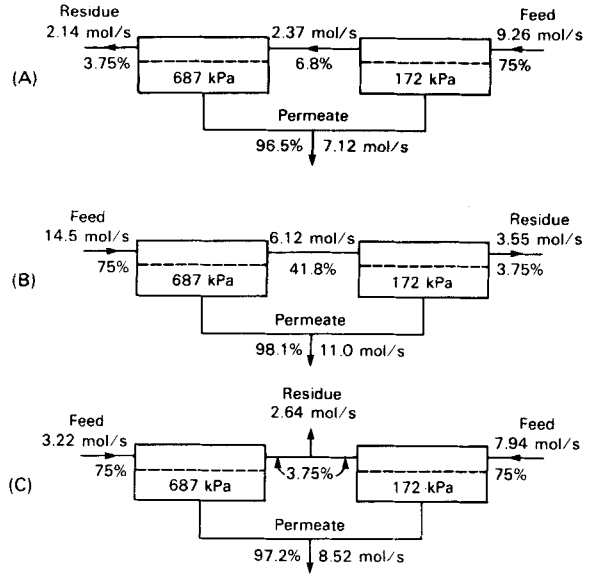

Figure 3. Effect of permeate-pressure variation along feed flow path on the performance of asymmetric membrane for gas separation. Calculated based on: $\alpha = 100$, $Q_b/d = 336$ pmol/m²·s·Pa, $P = 5{,}150$ kPa, 100 m²/permeator; calculation method by Weller and Steiner (1950a, b) or Pan and Habgood (1978a).

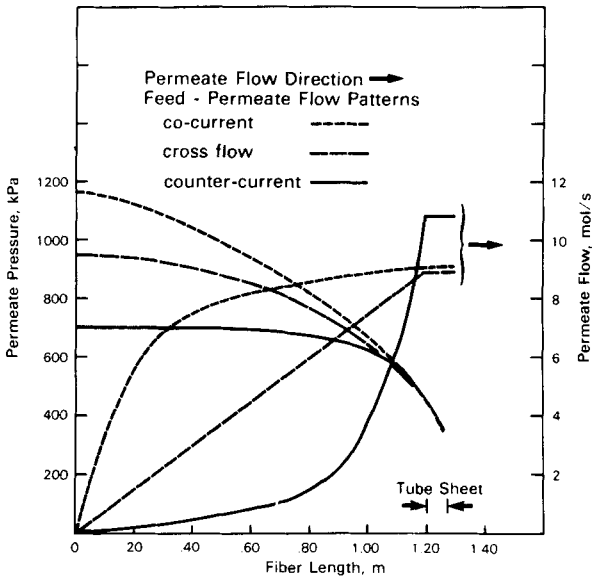

Figure 4. Effect of feed-permeate flow pattern on the permeate-pressure and permeate-flow profiles inside the bore of asymmetric hollow fibers. Calculated based on: He/CH_4 system, $\alpha = 100$, $D_l/D_l = 1.0$, $S_o/S_r = 1.056$, $A = 0.00191$ U_f^2, $S_r = 1.06/U_f$, T = 303 K, $P = 6{,}870$ kPa, $P_o = 344$ kPa, Feed = 60% He, Residue = 3% He.

higher permeate pressure. This is the least efficient operating mode as indicated by the permeate concentration and flow shown in the figure. Mode B, which operates with reversed feed flow, is the most efficient one. Mode C, in which each permeator is operated with the same feed and residue concentrations (but with different feed rates), has the intermediate gas separation performance. It is important to note that the discrete permeate pressure drop between the two permeators is countercurrent, cocurrent and cross-flow to the feed flow in Modes A, B and C, respectively. Mode B is the basis of a recent U.S. patent on membrane permeation processes by Graham and MacLean (1979). It is evident from the above discussion that for a given continuous permeate pressure profile in the permeator the unit operated with the feed flow cocurrent to the permeate pressure drop is the most efficient one, and the unit with the countercurrent pattern is least efficient. Since permeate flows in the direction of pressure drop, it follows that *for a given permeate pressure profile* the preferred feed-permeate flow pattern is the cocurrent mode, with the countercurrent mode being the least desirable. This is completely opposite to the operation of symmetric membrane. This conclusion, however, is reached without taking into account the effect of flow pattern on the permeate pressure build-up which is considered in the following analysis.

Figure 4 shows the calculated permeate pressure and flow profiles inside the fiber of a hollow-fiber module operated in cocurrent, countercurrent and cross-flow patterns (using the calculation methods described above). The permeation system and module operating conditions are chosen to manifest the effect of flow pattern on the permeate pressure build-up. It is seen that the countercurrent mode has the lowest permeate pressure build-up inside the fiber. In this flow pattern, the feed gas with high concentration of highly permeable helium enters the module near the fiber tube sheet and, consequently, most of the permeate flow is generated by the short length of fiber near the fiber opening; the short flow path for the large volume of permeate is responsible for the low permeate pressure build-up. The cocurrent flow pattern, on the other hand, produces a large volume of permeate at a far distance from the permeate outlet, resulting in high permeate pressure build-up.

The results of the above discussions may be summarized as follows. The cocurrent flow pattern has the desirable direction of feed flow in relation to the permeate pressure build-up, but the pressure build-up is excessive. The countercurrent flow pattern, on the other hand, has the lowest permeate pressure build-up but the feed flow is in the undesirable direction in relation to the permeate pressure build-up. The cross-flow is intermediate on both accounts. The actual performance of the module for gas separation will depend on the combined effect of these two factors—the magnitude and the direction of the permeate pressure build-up. For the particular example given in Figure 4, the countercurrent pattern turns out to be the best (permeate concentration = 92.1%) due mainly to the low level of permeate pressure build-up. However, the cocurrent pattern, despite its high permeate pressure build-up, is still slightly better than the cross-flow pattern (permeate concentrations 90.7% vs. 90.4%) due mainly to the favorable feed flow direction in relation to the permeate pressure build-up. In general, the preferred flow pattern is found to be dependent on operating conditions. Table 1 shows the calculated performance of the same module in countercurrent and cocurrent flow patterns for various residue concentrations. It is seen that for low residue concentrations, the countercurrent flow pattern is preferred. For high residue concentrations, however, the cocurrent mode is slightly better than the countercurrent mode. For most permeation systems operated with moderate product recovery, the effect of flow pattern on the performance of the asymmetric membrane is found to be insignificant. This is in sharp contrast to the characteristic of the symmetric membrane.

TABLE 1. EFFECT OF FEED-PERMEATE FLOW PATTERN ON MODULE PERFORMANCE AT VARIOUS RESIDUE CONCENTRATIONS (MODULE SPECIFICATIONS AND OPERATING CONDITIONS ARE SHOWN IN FIGURE 4)

Residue Concentration, %	Permeate Concentration, %		Feed Processed mol/s, Module	
	Counter current	Cocurrent	Counter current	Cocurrent
0.03	92.11	90.67	16.98	14.08
.06	94.14	93.71	22.64	20.42
.085	95.12	95.14	26.88	25.82
.12	96.02	96.27	32.56	32.88
.24	97.54	97.72	52.48	53.82
.48	98.63	98.66	150.94	151.60

EXPERIMENTAL RESULTS

The above theoretical study is only part of a large research program for the development of a membrane permeation process

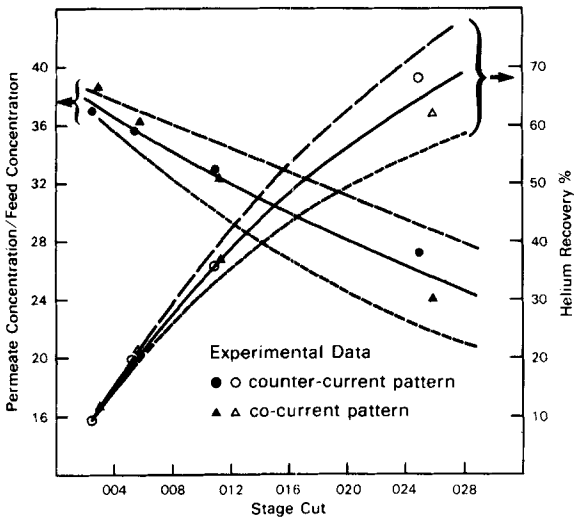

Figure 5. Effect of feed-permeate flow pattern on the performance of a small laboratory asymmetric fiber module for helium recovery from natural gas at various stage cuts (permeate flow/feed flow). System parameters: α = 190, D_t/D_l = 1.0, S_o/S_r = 1.25, $A = 4.24 \times 10^6\ U_f^2$, $S_r = 1.50 \times 10^{-6}/U_f$, T = 295 K, γ_o = 0.0177, Feed = 0.82% He. --- Calculated by assuming *symmetric* fiber in cocurrent flow pattern using the method described by Pan and Habgood (1978b). – – Calculated by assuming *symmetric* fiber in countercurrent flow pattern using the method described by Pan and Habgood (1978b). — Calculated by the present method for the *asymmetric* fiber in countercurrent, cocurrent or cross-flow pattern.

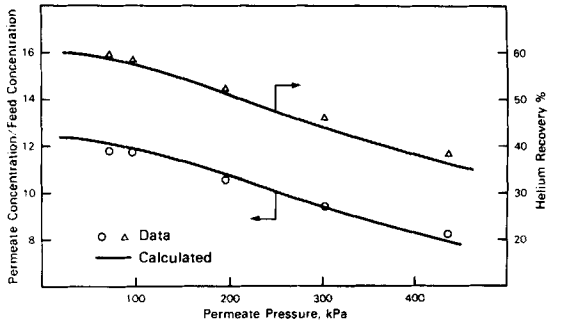

Figure 6. Comparison of calculated and observed performances of a large asymmetric fiber membrane module (220 m²) for helium recovery from pipeline natural gas at various permeate outlet pressures. System parameters: α = 95, D_t/D_l = 0.624, S_o/S_r = 1.056, A = 1.15, S_r = 0.0496, T = 303 K, P = 5,210 kPa, Feed = 0.085% He. Cross-flow pattern.

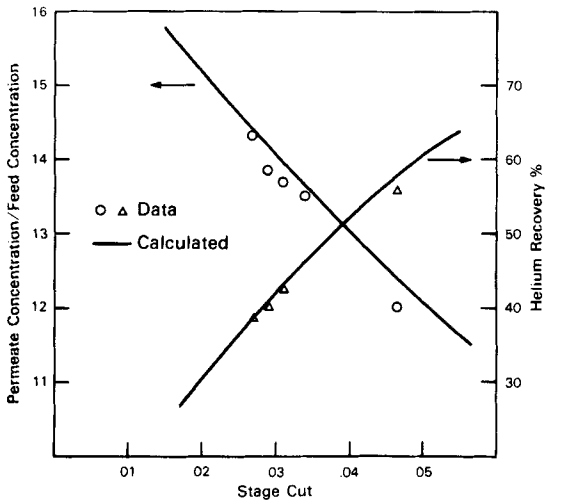

Figure 7. Comparison of calculated and observed performances of a large asymmetric fiber-membrane module for helium recovery from pipeline natural gas at various stage cuts (permeate flow/feed flow). System parameters: α = 98, D_t/D_l = 0.624, S_o/S_r = 1.056, $A = 0.0187\ U_f^2$, $S_r = 0.371/U_f$, T = 301 K, γ_o = 0.0191, Feed = 0.065% He. Cross-flow pattern.

for the recovery of helium from natural gas. Both laboratory and pilot-scale experiments using asymmetric membranes have been carried out to develop the process. The detailed test results will be published at a later date. Only very limited module performance data are presented here for the purpose of evaluating the mathematical model presented above.

In the laboratory, helium recovery experiments were performed on a small hollow-fiber permeator. The unit consists of a bundle of asymmetric fibers assembled inside a small copper tube with an epoxy tube sheet potted on both ends. Its structure is similar to the shell and tube heat exchanger. The high-pressure natural gas flows in the shell side and the permeate is withdrawn from the fiber openings in the tube sheet. The direction of feed or permeate flow can be reversed to yield countercurrent or cocurrent flow pattern. The experimental procedure is straightforward and the gas compositions were analyzed by gas chromatograph. The test results are shown in Figure 5. The helium enrichment and recovery as a function of stage cut (permeate/feed flow ratio) were investigated for both countercurrent and cocurrent flow patterns. The membrane performance curves calculated by the mathematical models for both asymmetric and symmetric fibers are also shown in the figure for comparison with the data. (The calculation method for the symmetric hollow fiber has been reported by Pan and Habgood, 1978b.) The model based on the symmetric fiber predicts a significant effect of flow pattern on module performance, which is clearly not substantiated by the test results. The mathematical model presented in this paper for the asymmetric fiber, on the other hand, predicts a virtually identical performance for both flow patterns, which appears to be confirmed by the experimental data. The small difference of experimental data between the countercurrent and cocurrent flow patterns may be mainly due to experimental errors (estimated to be around 4%). This is based on the observation that the data difference at the low stage-cut regions seems to increase with decreasing stage cut. Such a variation is not consistent with the fact that for any type of membrane (asymmetric or symmetric) the effect of flow pattern on membrane performance should diminish with decreasing stage cut due to increased uniformity of the feed-side concentration resulting from increased feed flow rate.

The somewhat larger difference of the data between the two flow patterns at stagecut of around 0.025, however, cannot be totally accounted for by the experimental errors. A preliminary analysis indicates that it is due to the effect of back diffusion along the pore path in the porous supporting layer. This is because the membrane used in this particular experiment has only moderately high permeabilities (Q_b/d = 60.5 pmol/m²·s·Pa and α = 190). The permeate velocity through the porous layer is not high enough to totally overcome the effect of pore diffusion (molecular and Knudson) due to large difference between y' and y arising from high stage-cut operation. Such diffusion will tend to dilute and concentrate the permeate concentration on the membrane skin surface for the countercurrent and cocurrent patterns, respectively, resulting in the observed difference of the membrane performance shown in Figure 5. A detailed analysis of the effect of pore diffusion will require the knowledge of pore structure of the membrane and will be dealt with in a separate paper with additional data. Here it may be noted that an asymmetric membrane with low permeate flux or a thin porous layer may behave like a symmetric membrane.

In the field, a large multistage pilot plant was used to conduct feld tests of large asymmetric fiber modules (220 m²/unit) for helium recovery from pipeline natural gas. The permeability of the fiber is about five times that of the membrane used in the laboratory experiments. The details of the pilot-plant project, including module properties and specifications, may be cleared for publication at a later date. Figures 6 and 7 give the typical test results obtained from the first permeation stage of the pilot plant

showing the effects of permeate pressure and stage cut on module performance. The curves in the figures are calculated by the present model for the asymmetric membrane using laboratory helium and methane permeability data of fiber samples. The calculated values are in good agreement with the experimental data.

ACKNOWLEDGMENT

This work was supported by Alberta Helium Ltd., Calgary, Alberta, which is owned by the Government of Alberta, TransCanada Pipelines Ltd., and Alberta and Southern Gas Co.

NOTATION

A = dimensionless constant defined by Eq. 17
B = permeability of the spacing materials inside the membrane leaf of a spiral-wound module, m^2
c = dimensionless constant defined by Eq. 33
d = effective skin thickness of asymmetric membrane, m
D_i = hollow fiber inside diameter, m
D_o = hollow fiber outside diameter, m
D_t = inside diameter of the fiber imbedded in the tube sheet, m
g_c = Newton's law conversion factor
h = l/L, membrane leaf length variable of spiral-wound module measured from the closed end, dimensionless
l = hollow fiber length variable or membrane leaf length variable measured from the closed end, m
l_r = active fiber length, m
l_o = total fiber length (active length + inactive length inside the tube sheet), m
L = membrane leaf length of spiral-wound module, m
N = total number of active fibers in the hollow-fiber module
P = feed-side pressure, Pa
p = permeate-side pressure, Pa
p_o = permeate outlet pressure, Pa
p_r = permeate pressure at the junction of active fiber and the tube sheet, Pa
Q_a = permeability of the more permeable component, mol/m·s·Pa
Q_b = permeability of the less permeable component, mol/m·s·Pa
R = ideal gas constant
S = $\pi D_o l N(Q_b/d)(P/U_f)$, membrane area variable, dimensionless
S_o = $\pi D_o l_o N(Q_b/d)(P/U_f)$, total membrane area (active + inactive), dimensionless
S_r = $\pi D_o l_r N(Q_b/d)(P/U_f)$, total active membrane area, dimensionless
t = membrane leaf thickness, m
T = temperature, K
u = feed-side gas flow rate per unit length of membrane leaf or hollow fiber in cross-flow mode, mol/s, m
u_f = feed gas flow rate per unit length of membrane leaf or hollow fiber in cross-flow mode, mol/s·m
u_r = residue gas flow rate per unit length of membrane leaf or hollow fiber in cross-flow mode, mol/s, m
U = feed-side gas flow rate per hollow-fiber module or per membrane leaf of spiral-wound module, mol/s
U_f = feed gas flow rate per hollow-fiber module in cocurrent flow pattern or per membrane leaf of spiral-wound module, or residue flow rate (negative) per hollow-fiber module in countercurrent flow pattern, mol/s
U_r = residue gas flow rate per hollow-fiber module in cocurrent flow pattern or per membrane leaf of spiral-wound module, or feed flow rate (negative) per hollow-fiber module in countercurrent flow pattern, mol/s
V = permeate flow rate, mol/s
V_o = permeate flow rate at permeate outlet, mol/s
V_r = permeate flow rate at fiber opening, mol/s
w = membrane leaf width variable measured from the feed inlet end, m
W = membrane leaf width, m
x = feed-side concentration, mol fraction
x_f = feed concentration for cocurrent and cross-flow patterns, or residue concentration for countercurrent flow pattern, mol fraction
x_r = residue concentration for cocurrent and cross-flow patterns, or feed concentration for countercurrent flow pattern
y' = local permeate concentration on the membrane surface, mol fraction
y'_f = permeate concentration on the membrane surface at the closed end of the fiber, or at the feed inlet end of the membrane leaf, mol fraction
y'_r = permeate concentration on the membrane surface at the junction of active fiber and tube sheet or at the residue outlet end of the membrane leaf, mol fraction
y = permeate concentration in the bulk permeate stream, mol fraction
y_o = average permeate concentration in the bulk permeate stream at the permeate outlet, mol fraction
y_r = permeate concentration in the bulk permeate stream at fiber opening, mol fraction
α = membrane selectivity (permeability of more permeable component/permeability of less permeable component)
γ = ratio of permeate pressure to feed pressure
γ_f = ratio of permeate pressure to feed pressure at the closed end of the fiber
γ_o = ratio of permeate pressure to feed pressure at the permeate outlet
γ_r = ratio of permeate pressure to feed pressure at the junction of the active fiber and the tube sheet
μ = viscosity of a gas mixture, Pa·s
μ_b = viscosity of the less permeable component, Pa·s
μ_r = viscosity of the permeate stream at the fiber opening, Pa·s
θ = ratio of permeate flow to feed flow
θ_o = ratio of permeate flow to feed flow at permeate outlet

LITERATURE CITED

Berman, A. S., "Laminar Flow in Channels with Porous Walls," *J. Appl. Phys.*, **24**, p. 1232 (1953).

Blaisdell, C. T., and K. Kammermeyer, "Gas Separation through Expansible Tubing," *AIChE J.*, **18**, p. 1015 (1972).

Blaisdell, C. T., and K. Kammermeyer, "Counter-current and Co-current Gas Separation," *Chem. Eng. Sci.*, **28**, p. 1249 (1973).

Graham, T. E., and D. L. MacLean, "Processes," U.S. Patent 4,180,388 (1979).

Hwang, S. T., and K. Kammermeyer, "Membranes in Separations," Wiley-Interscience, New York (1975).

Naylor, R. W., and P. O. Backer, "Enrichment Calculations in Gaseous Diffusion: Large Separation Factor," *AIChE J.*, **1**, p. 95 (1955).

Oishi, J., Y. Matsumura, K. Higashi, and C. Ika, "Analysis of A Gaseous Diffusion Separation Unit," *J. Atomic Energy Soc. (Japan)*, **3**, p. 923 (1961); U.S. Atomic Energy Commission Report AEC-TR-5134.

Pan, C. Y., and H. W. Habgood, "An Analysis of the Single-Stage Gaseous Permeation Process," *Ind. Eng. Chem. Fund.*, **13**, p. 323 (1974).

Pan, C. Y., and H. W. Habgood, "Gas Separation by Permeation. Part I. Calculation Methods and Parametric Analysis," *Can. J. Chem. Eng.*, **56**, p. 197 (1978a).

Pan, C. Y., and H. W. Habgood, "Gas Separation by Permeation. Part II. Effect of Permeate Pressure Drop and Choice of Permeate Pressure," *Can. J. Chem. Eng.*, **56**, p. 210 (1978b).

Stern, S. A., in "Industrial Processing with Membranes," Lacey, R. E. and S. Leob, Eds., Wiley-Interscience, New York (1972).
Thorman, J. M., H. Rhim, and S-T Hwang, "Gas Separation by Diffusion through Silicone Rubber Capillaries," *Chem. Eng. Sci.*, **30**, p. 751 (1975).
Walawender, W. P., and S. A. Stern, "Analysis of Membrane Separation Parameters: II. Countercurrent and Cocurrent Flow in a Single Permeation Stage," *Separation Sci.*, **7**, p. 553 (1972).
Weller, S., and W. A. Steiner, "Separation of Gases by Fractional Permeation through Membrane," *J. Appl. Phys.*, **21**, p. 279 (1950a).
Weller, S., and W. A. Steiner, "Engineering Aspects of Separation of Gases—Fractional Permeation through Membranes," *Chem. Eng. Prog.*, **46**, p. 585 (1950b).

Manuscript received March 29, 1982; revision received August 11, and accepted August 30, 1982.

Multiplicity Criteria for Multireaction Networks

VEMURI BALAKOTAIAH and DAN LUSS

Department of Chemical Engineering
University of Houston
Houston, TX 77004

A general method is developed for a systematic determination of criteria predicting steady-state multiplicity in lumped-parameter systems in which many irreversible reactions occur simultaneously. The method enables use of criteria derived for simple reaction networks to predict the behavior of more complex networks. The available multiplicity criteria for the single- and two-reaction networks can always be used to write down sufficient multiplicity criteria for any multireaction system. Several examples illustrate the power of the proposed technique.

SCOPE

Most practical control and start-up problems associated with steady-state multiplicity are encountered in systems in which several chemical reactions occur simultaneously and are due to the "taking over" by an undesired reaction, whose rate is negligible at the normal operating conditions. It is of practical and academic interest to have simple criteria predicting in terms of simple observable quantities the conditions for which multiplicity exists in multireaction systems. At present exact criteria are available only for predicting the conditions under which multiplicity exists in a lumped-parameter system in which either a single or two chemical reactions occur (Aris, 1969; Michelsen, 1977; Balakotaiah and Luss, 1982a).

The steady-state equation describing N first-order reactions occurring in a lumped-parameter system is of the form

$$F(y,p^*,Da) = 0$$

where y is the dimensionless temperature, p^* is a vector of parameters and Da is a vector of N Damköhler numbers. The large number of parameters and the highly nonlinear nature of the steady-state equation prevent, in general, a direct prediction if multiplicity occurs for some p^* and Da. Instead, we suggest to derive first criteria predicting the conditions that p^* has to satisfy so that multiplicity occurs for some Da. When at least one of these criteria is satisfied we can construct the exact boundaries of the multiplicity region and check if the specific Da is within the region.

The goal of this work is to reveal the structure of the criteria that guarantee multiplicity for some Da and to present a systematic method of determining them for any chemical reaction network. Moreover, we show how the available criteria for simple reaction networks can be utilized to predict multiplicity of more complex reaction networks.

CONCLUSIONS AND SIGNIFICANCE

When N reactions occur in a lumped-parameter system, the conditions that the parameter vector p^* has to satisfy so that multiplicity exists for some Da, can be derived by analyzing systematically the limiting cases in which only j reactions proceed at a finite rate while each of the remaining $N - j$ reactions is either instantaneous ($Da_i \to \infty$) or occurs at a negligible rate ($Da_i = 0$). This scheme generates at most $3^N - 2^N$ multiplicity criteria, some of which are implied by others and can be discarded. This procedure enables one to incorporate in the analysis of any multireaction network all the available criteria about simpler reaction networks. Thus, the available criteria for the single- and two-reaction cases can always be utilized to write down some sufficient multiplicity criteria for any multireaction network. A simple scheme is derived for determining the boundaries of the multiplicity region for the case that it exists for some Da. The procedure described here is expected to become the standard tool for predicting multiplicity in multireaction systems.

Three examples are used to illustrate the application of the technique to different multireaction networks. These examples led to the derivation of simple necessary and sufficient conditions predicting when multiplicity exists for some Da in the case of N simultaneous or parallel reactions. It is proven that when N simultaneous first-order reactions occur in a CSTR multiplicity can occur for some Da if and only if it can exist when only two of the N reactions occur.